AAS 12-129

DESIGN OF SPACECRAFT MISSIONS TO TEST KINETIC IMPACT FOR ASTEROID DEFLECTION

Sonia Hernandez* **and Brent W. Barbee†**

Earth has previously been struck with devastating force by near-Earth asteroids (NEAs) and will be struck again. Telescopic search programs aim to provide advance warning of such an impact, but no techniques or systems have yet been tested for deflecting an incoming NEA. To begin addressing this problem, we have analyzed the more than 8000 currently known NEAs to identify those that offer opportunities for safe and meaningful near-term tests of the proposed kinetic impact asteroid deflection technique. In this paper we present our methodology and results, including complete mission designs for the best kinetic impactor test mission opportunities.

INTRODUCTION

There are currently 8469 known near-Earth asteroids (NEAs), and more are being discovered on a continual basis. Of these, 1276 are classified as Potentially Hazardous Asteroids (PHAs)[‡] because their Minimum Orbit Intersection Distance (MOID) with Earth's orbit is ≤ 0.05 AU and their estimated diameters are ≥ 150 m[§]. To date, 182 confirmed Earth impact structures[¶] have been discovered, with hundreds more under investigation. These discoveries demonstrate that our planet has previously been struck with devastating force by NEAs and will be struck again. Such collisions are aperiodic events and can occur at any time.

A variety of techniques have been suggested to defend our planet from NEA impacts by deflecting the incoming NEA.[1–3] However, none of these techniques have been tested. Unless rigorous testing is conducted to produce reliable NEA deflection systems, we will be forced to deploy a completely untested—and therefore unreliable—deflection mission when a sizable NEA on a collision course with Earth is discovered. Such a mission will have a high probability of failure.

We propose to address this problem with a campaign of deflection technology test missions deployed to harmless NEAs. The objective of these missions is to safely evaluate and refine the mission concepts and NEA deflection system designs. Our current research focuses on the kinetic impactor, one of the simplest proposed NEA deflection techniques in which a spacecraft is sent

*Graduate Student, Department of Aerospace Engineering and Engineering Mechanics, The University of Texas at Austin, Austin, TX, 78712, USA, sonia.hernandez@utexas.edu.

†Aerospace Engineer, NASA GSFC, Code 595, 8800 Greenbelt Road, Greenbelt, MD 20771, USA, Member AIAA brent.w.barbee@nasa.gov.

‡NEA population statistics, including the total number of known NEAs and the number of those that are classified as PHAs, are updated daily at http://neo.jpl.nasa.gov/stats/. Last accessed on 01/09/2012.

§http://neo.jpl.nasa.gov/neo/groups.html. Last accessed on 01/09/2012.

¶http://www.passc.net/EarthImpactDatabase/index.html. Last accessed on 01/09/2012.

to collide with a NEA at high relative velocity, thereby changing the NEA's momentum and subsequent heliocentric orbit. By deploying test missions in the near future, we can characterize the performance of this deflection technique and resolve any problems inherent to its execution before needing to rely upon it during a true emergency.

We first identify the subpopulation of NEAs whose orbits lie either entirely outside or inside Earth's orbit. By choosing NEAs for the proposed test missions whose orbits do not cross Earth's orbit, we ensure that Earth will never be threatened by test activities, regardless of what might go wrong during a deflection test mission. We also seek low Δv missions for the sake of affordability, and therefore only selected NEAs with heliocentric orbit inclination $\leq 20^{\circ}$ for this study. Besides safety and affordability, an additional constraint is that the deflection imparted to the NEA by the kinetic impactor must be easily measured by an observer spacecraft that has rendezvoused with the NEA prior to the collision of the kinetic impactor. To ensure a measurable experiment, we require that the difference in position between the NEA's deflected and undeflected orbits reach at least 100 km by 2 years after impact.

We surveyed the aforementioned NEA subpopulation using three simulated mission design concepts. In the first case, the observer and impactor spacecraft are launched separately on two launch vehicles. In the second case, the observer and impactor launch together on one launch vehicle into an Earth escape trajectory that takes the observer directly to rendezvous with the NEA. The impactor separates from the observer after launch but before observer arrival at the NEA by performing a maneuver such that it will collide with the NEA after the observer has spent adequate time gathering data on the NEA. In the third case, the observer and impactor launch together on one launch vehicle into Low Earth Orbit (LEO) and then depart LEO at different times. In all cases, we enforced the constraint that the observer spacecraft must arrive between 3 months and 3 years prior to the impactor's collision with the NEA.

In this paper we present the methodology and results of our survey, including lists of NEAs for which safe and effective kinetic impactor test missions may be conducted during the coming decade. Detailed trajectory design results for selected NEAs are also presented.

IMPULSIVE KINETIC IMPACTOR MODEL

A kinetic impactor imparts an impulsive velocity change to a NEA by colliding a spacecraft with the NEA in a controlled manner. The principle of conservation of linear momentum holds during the impact and a purely plastic collision is assumed, which means that the spacecraft does not bounce off the NEA after the collision. In this section we develop a model to compute the change in velocity imparted to the NEA.

A simple model to estimate the change in a NEA's momentum due to an impact from a spacecraft is presented in Ref. 1. The model assumes that the spacecraft impacts the NEA along the NEA's velocity direction. This assumption is restrictive because it does not apply to the more general scenario in which the the impacting spacecraft may approach the NEA from any angle. We build upon the previous work by developing a model to compute the change in a NEA's momentum due to a spacecraft collision with any impact angle in three-dimensional space relative to the NEA, i.e., the spacecraft may approach the NEA with any combination of azimuth angle, α, and elevation angle, δ, as shown in Figure 1(a).

Assume that immediately before the time of impact t_{imp} the NEA's position and velocity ex-

pressed the Heliocentric Inertial (HCI) frame are $\mathbf{r}_{nea}^-$ and $\mathbf{v}_{nea}^-$, respectively.* The state of the impacting spacecraft is given by its inertial position and velocity as $\mathbf{r}_{sc}^-$ and $\mathbf{v}_{sc}^-$. Immediately after the collision, the velocity of the NEA and spacecraft are $\mathbf{v}_{nea}^+$ and $\mathbf{v}_{sc}^+$, respectively, while the position vectors of the NEA and the spacecraft are unchanged, i.e., $\mathbf{r}_x^- = \mathbf{r}_x^+ = \mathbf{r}_x$, where x denotes nea or sc.

The Radial, In-Track, Cross-Track (RIC) Frame

Figure 1(a) shows the applied impulsive velocity change $\mathbf{\Delta v}$ in the NEA's Radial, In-Track, Cross-Track (RIC) frame at the time of collision, where the RIC frame basis vectors are denoted as $\hat{\mathbf{r}}$, $\hat{\mathbf{i}}$, and $\hat{\mathbf{c}}$. The RIC frame will be used to model the change in momentum imparted on the NEA and its orthonormal basis vectors are computed as

$$\hat{\mathbf{r}} = \frac{\mathbf{r}_{nea}}{\|\mathbf{r}_{nea}\|} \qquad \hat{\mathbf{c}} = \frac{\mathbf{r}_{nea} \times \mathbf{v}_{nea}^-}{\|\mathbf{r}_{nea} \times \mathbf{v}_{nea}^-\|} \qquad \hat{\mathbf{i}} = \hat{\mathbf{c}} \times \hat{\mathbf{r}} \tag{1}$$

The matrix that transforms vectors from the inertial frame to the RIC frame is thus constructed as

$$T_I^{RIC} = \begin{bmatrix} \hat{r}_1 & \hat{r}_2 & \hat{r}_3 \\ \hat{i}_1 & \hat{i}_2 & \hat{i}_3 \\ \hat{c}_1 & \hat{c}_2 & \hat{c}_3 \end{bmatrix} \tag{2}$$

where the numbered subscripts denote the components of each basis vector. The velocity of the NEA expressed in its RIC frame is $\mathbf{v}_{nea_{RIC}}^- = T_I^{RIC}\mathbf{v}_{nea}^-$. Note that the velocity of the NEA lies in the RI-plane and its C component is therefore always zero. Alternatively, the velocity of the NEA in the RIC frame can be expressed as a function of its norm† and the flight path angle ϕ,

$$\begin{aligned} \mathbf{v}_{nea_{RIC}}^- &= T_I^{RIC}\mathbf{v}_{nea}^- \\ &= v_{nea}^- \begin{pmatrix} \sin\phi \\ \cos\phi \\ 0 \end{pmatrix}. \end{aligned} \tag{3}$$

where ϕ is defined in Figure 1(a) as the angle between the NEA's velocity vector and the In-Track axis $\hat{\mathbf{i}}$. The velocity of the spacecraft at the time of impact can be parametrized by its magnitude, $v_{sc}^- = \|\mathbf{v}_{sc}^-\|$, and two spherical coordinate angles α and δ, which are the azimuth and elevation angles, respectively, measured in the RIC frame as shown in Figure 1(a).

$$\mathbf{v}_{sc_{RIC}} = v_{sc}^- \begin{pmatrix} \cos\alpha\cos\delta \\ \sin\alpha\cos\delta \\ \sin\delta \end{pmatrix} \tag{4}$$

To model the change in momentum, we assume that a spherical spacecraft impacts a spherical NEA such that the line of impact connects the centers of mass of the spacecraft and the NEA. We begin by discussing a simple model,[1] in which the spacecraft impacts along the velocity direction of the NEA, and work towards a more complicated general model in which the spacecraft impacts the NEA along any direction.

*Note that any vector $\mathbf{x}$ expressed in this paper resides in three dimensions, $\mathbf{x} \in \mathbb{R}^3$.

†The 2-norm of any vector $\mathbf{x} \in \mathbb{R}^3$ is denoted by $x = \|\mathbf{x}\|$.

Impact in the NEA Orbit Plane

Assume that the spacecraft intercepts the NEA at perihelion parallel to the NEA's velocity vector, i.e. $\phi = 0°$, $\alpha = 90°$, and $\delta = 0°$. At perihelion the NEA's velocity vector lies along the In-Track axis* such that $\mathbf{v}^-_{nea_{RIC}} = v^-_{nea}\hat{\mathbf{i}}$ and the spacecraft impacts the NEA with a velocity $\mathbf{v}^-_{sc_{RIC}} = v^-_{sc}\hat{\mathbf{i}}$. Because it is a plastic collision, the velocity of the spacecraft and NEA will be the same after collision. In the RIC frame,

$$\mathbf{v}^+_{sc_{RIC}} = \mathbf{v}^+_{nea_{RIC}} = v^+_{nea}\hat{\mathbf{i}}, \tag{5}$$

where $v^+_{nea} = \|\mathbf{v}^+_{nea}\|$. We make the assumption that no external forces act upon the NEA-spacecraft system at the instant of impact, such that linear momentum is conserved in the $\hat{\mathbf{i}}$ direction, i.e.,

$$mv^-_{sc} + Mv^-_{nea} = (m + M)v^+_{nea} \tag{6}$$

where m is the mass of the spacecraft and M is the mass of the NEA. Solving for v^+_{nea} from Eq. (6) and subtracting it from v^-_{nea}, the change in velocity imparted to the NEA is

$$\boldsymbol{\Delta}\mathbf{v} = \Delta v\hat{\mathbf{i}} = \beta\frac{m}{m+M}\left[v^-_{sc} - v^-_{nea}\right]\hat{\mathbf{i}} \tag{7}$$

where β is as the *impact efficiency factor*, or *momentum scaling factor*. One impetus for the deflection system tests we propose in this paper is that β is currently poorly characterized. Current consensus on the range for this parameter is $1 \leq \beta \leq 5$.[4,5] $\beta = 1$ corresponds to a perfectly plastic collision in which the impacting spacecraft is absorbed and no ejecta is produced from the impact crater. $\beta = 2$ corresponds to a perfectly elastic collision in which the momentum of the ejecta is equal and opposite to the momentum of the impactor and $\beta > 2$ corresponds to a super-elastic collision.

We now assume that a spacecraft impacts a NEA with any azimuth angle, α, at any point along the NEA's orbit, such that the NEA will therefore have a (generally) non-zero flight path angle, ϕ. However, we restrict the impact to occur at zero elevation ($\delta = 0°$), i.e., the line of impact lies entirely in the RI-plane. When the spacecraft impacts the NEA it applies an external force on the NEA in the direction of the impacting spacecraft's velocity. Linear momentum is conserved for the spacecraft-NEA system, but only along the direction of the spacecraft's velocity, which we refer to as the line of impact, depicted as the dashed line in Figure 1(b). For that reason, a body-frame B with basis vectors $\hat{\mathbf{b}}_1$, $\hat{\mathbf{b}}_2$, and $\hat{\mathbf{b}}_3$ is defined whose origin is at the center of mass of the NEA. The $\hat{\mathbf{b}}_1$ axis points in the direction of the spacecraft's velocity vector, $\mathbf{v}^-_{sc_{RIC}}$, $\hat{\mathbf{b}}_3$ is parallel to the $\hat{\mathbf{c}}$ axis of the RIC frame, and $\hat{\mathbf{b}}_2$ completes the right-handed set.

Because the collision is plastic, the components of the spacecraft and NEA velocities along the line of impact $\hat{\mathbf{b}}_1$ will be the same after impact, $v^+_{nea_{\hat{b}_1}} = v^+_{sc_{\hat{b}_1}}$. Further, because the impulse only occurs along $\hat{\mathbf{b}}_1$, the velocity components of the spacecraft and NEA along the $\hat{\mathbf{b}}_2$ and $\hat{\mathbf{b}}_3$ directions will not change due to the collision, such that $v^-_{nea_{\hat{b}_2}} = v^+_{nea_{\hat{b}_2}}$ and $v^-_{nea_{\hat{b}_3}} = v^+_{nea_{\hat{b}_3}}$. Consequently, the NEA's velocity change is confined to the $\hat{\mathbf{b}}_1$ axis, $\boldsymbol{\Delta}\mathbf{v}_B = \Delta v\ \hat{\mathbf{b}}_1$, where Δv is

$$\Delta v = \beta\frac{m}{m+M}\left[v^-_{sc} - v^-_{nea}\sin(\phi + \alpha)\right] \tag{8}$$

*This is true for the case of a NEA with an eccentric heliocentric orbit; the velocity vector would always lie along the In-Track axis for the case of a perfectly circular orbit, but these are exceedingly rare in nature.

Note that the last term in Eq. (8) corresponds to the NEA's velocity component in the $\hat{\mathbf{b}}_1$ axis before the impact.

$$\begin{aligned} v^-_{nea_{\hat{b}_1}} &= \cos\alpha\, v^-_{nea_{\hat{r}}} + \sin\alpha\, v_{nea_{\hat{i}}} \\ &= (\cos\alpha\sin\phi + \sin\alpha\cos\phi)\, v^-_{nea} \\ &= \sin(\alpha+\phi) v^-_{nea} \end{aligned} \tag{9}$$

After transforming to the RIC frame, the change in velocity becomes

$$\mathbf{\Delta v}_{RIC} = \Delta v \begin{pmatrix} \cos\alpha & \sin\alpha & 0 \end{pmatrix}^T \tag{10}$$

Finally, the inertial velocity of the NEA after the impact is computed using the T_I^{RIC} matrix provided in Eq. (2) as follows

$$\mathbf{v}^+_{nea} = \mathbf{v}^-_{nea} + (T_I^{RIC})^T \mathbf{\Delta v}_{RIC} \tag{11}$$

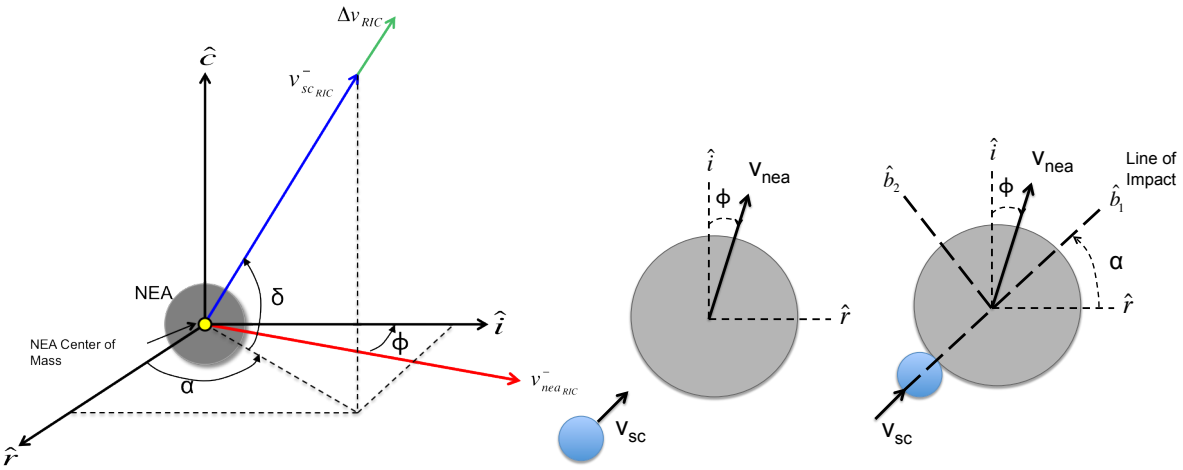

(a) Impact on NEA with $\delta \neq 0$ (b) Impact on NEA with $\delta = 0$

Figure 1. Change in Momentum Imparted to a NEA at the Time of Impact in the NEA's RIC Frame

Three Dimensional Impact

We now compute the change in the NEA's velocity for the most general case, in which the impacting spacecraft approaches from any incoming azimuth and elevation and the NEA is at any point along its heliocentric orbit, with flight path angle ϕ, see Figure 1(a). As described previously, the linear momentum of the spacecraft-NEA system is conserved only along the line of impact, which coincides with the direction of the spacecraft's velocity. We again define a body-frame $B = (\hat{\mathbf{b}}_1, \hat{\mathbf{b}}_2, \hat{\mathbf{b}}_3)$, in which the $\hat{\mathbf{b}}_1$ axis points in the direction of the spacecraft's velocity vector, $\mathbf{v}^-_{sc_{RIC}}$. The B-frame basis vectors are formally defined according to

$$\hat{\mathbf{b}}_1 = \frac{\mathbf{v}^-_{sc_{RIC}}}{\|\mathbf{v}^-_{sc_{RIC}}\|} \qquad \hat{\mathbf{b}}_2 = \hat{\mathbf{b}}_3 \times \hat{\mathbf{b}}_1 \qquad \hat{\mathbf{b}}_3 = \frac{\mathbf{r}_{sc_{RIC}} \times \mathbf{v}^-_{sc_{RIC}}}{\|\mathbf{r}_{sc_{RIC}} \times \mathbf{v}^-_{sc_{RIC}}\|} \tag{12}$$

The transformation matrix from RIC to the body-frame B of the spacecraft is then constructed as

$$T^B_{RIC} = \begin{bmatrix} \hat{b}_{11} & \hat{b}_{12} & \hat{b}_{13} \\ \hat{b}_{21} & \hat{b}_{22} & \hat{b}_{23} \\ \hat{b}_{31} & \hat{b}_{32} & \hat{b}_{33} \end{bmatrix} \tag{13}$$

The velocity of the spacecraft in the body-frame therefore only has a component in the $\hat{\mathbf{b}}_1$ direction, which can be verified by

$$\mathbf{v}^-_{sc_B} = \begin{pmatrix} v^-_{sc} & 0 & 0 \end{pmatrix}^T = T^B_{RIC}\, T^{RIC}_I \mathbf{v}_{sc} \tag{14}$$

The velocity of the NEA in the body-frame is computed as

$$\mathbf{v}^-_{nea_B} = T^B_{RIC} T^{RIC}_I \mathbf{v}^-_{nea} \tag{15}$$

As stated previously, a consequence of the conservation of linear momentum is that the NEA experiences a change in velocity due to the impact only along the line of impact, which coincides with the $\hat{\mathbf{b}}_1$ axis.* Therefore, the change in velocity of the NEA expressed in the B frame is

$$\boldsymbol{\Delta}\mathbf{v}_B = \begin{pmatrix} \beta\frac{m}{m+M}(v^-_{sc_{\hat{b}_1}} - v^-_{nea_{\hat{b}_1}}) & 0 & 0 \end{pmatrix}^T \tag{16}$$

where $v^-_{sc_{\hat{b}_1}}$ and $v^-_{nea_{\hat{b}_1}}$ are the first components of the spacecraft and NEA velocities in the B frame. We can now determine the inertial change in velocity vector for the NEA as follows

$$\boldsymbol{\Delta}\mathbf{v} = (T^{RIC}_I)^T (T^B_{RIC})^T \boldsymbol{\Delta}\mathbf{v}_B \tag{17}$$

The inertial velocity of the NEA after the impact is therefore given by

$$\mathbf{v}^+_{nea} = \mathbf{v}^-_{nea} + \boldsymbol{\Delta}\mathbf{v} \tag{18}$$

Optimal Impact Angle for Maximum Impulse

An analytical expression for the optimal impact angle to obtain maximum impulse is derived for the specific case when the elevation angle, δ, of the spacecraft's impact direction is zero, i.e., $\delta = 0^\circ$, and the impact occurs at the NEA's perihelion such that $\phi = 0^\circ$. In this case the NEA's velocity prior to impact is entirely along the In-Track axis. The velocity of the NEA after impact under these conditions is given by

$$\mathbf{v}^+_{nea_{RIC}} = \begin{pmatrix} \Delta v \cos\alpha \\ v^-_{nea} + \Delta v \sin\alpha \\ 0 \end{pmatrix} \tag{19}$$

where Δv is given by Eq. (8) with $\phi = 0^\circ$.

The goal is to maximize the NEA's final velocity, which is equivalent to maximizing the square of it's velocity,

$$\begin{aligned} \max_\alpha\ J &= \|\mathbf{v}^+_{nea}\|^2 \\ &= (\Delta v \cos\alpha)^2 + \left(v^-_{nea} + \Delta v \sin\alpha\right)^2 \\ &= {v^-_{nea}}^2 + \Delta v^2 + 2\Delta v v^-_{nea} \sin\alpha \end{aligned} \tag{20}$$

The optimal solution is found by taking the derivative of J with respect to the impact angle α,

$$\begin{aligned} \frac{dJ}{d\alpha} &= 2\Delta v \frac{d}{d\alpha}(\Delta v) + 2\Delta v v^-_{nea}\cos\alpha + 2v^-_{nea}\sin\alpha\frac{d}{d\alpha}(\Delta v) \\ &= 2v_{nea}\cos\alpha\left[\Delta v - \beta\frac{m}{m+M}\left(\Delta v + v^-_{nea}\sin\alpha\right)\right] = 0 \end{aligned} \tag{21}$$

*Recall that there can be no change in momentum along either of the other two B-frame axes because no external forces are acting upon the spacecraft-NEA system.

where $\frac{d}{d\alpha}(\Delta v) = -\beta\frac{m}{m+M}v_{nea}^{-}\cos\alpha$. One optimal solution occurs when $\cos\alpha = 0$, which corresponds to $\alpha = 90^\circ$ (a local minimum). Note that $\alpha = 270^\circ$ is also an optimal solution, but corresponds to a retrograde heliocentric orbit for the spacecraft, which is impractical. The other optimal solution, which corresponds to a local maximum, occurs when

$$\Delta v - \beta\frac{m}{m+M}\left(\Delta v + v_{nea}\sin\alpha\right) = 0 \Rightarrow \sin\alpha = \frac{1-\beta\frac{m}{m+M}}{2-\beta\frac{m}{m+M}}\frac{v_{sc}^{-}}{v_{nea}^{-}} \tag{22}$$

As a limiting case, when the spacecraft reaches the NEA with zero relative velocity and assuming $\beta = 1$, the optimal impact angle occurs at $\alpha = 30^\circ$ and 150°. As the relative velocity between the spacecraft and the NEA increases, the optimal impact ceases to be double-valued, converging to a single optimal impact angle at $\alpha = 90^\circ$. These behaviors are shown in Figure 2(a), where each curve represents Δv as a function of α for different velocities of a spacecraft of mass $m = 5\cdot10^3$ kg relative to an NEA of mass $M = 10^9$ kg. The contour plot in Figure 2(b) shows a similar behavior, using a mass value for the NEA of $M = 10^{10}$ kg.

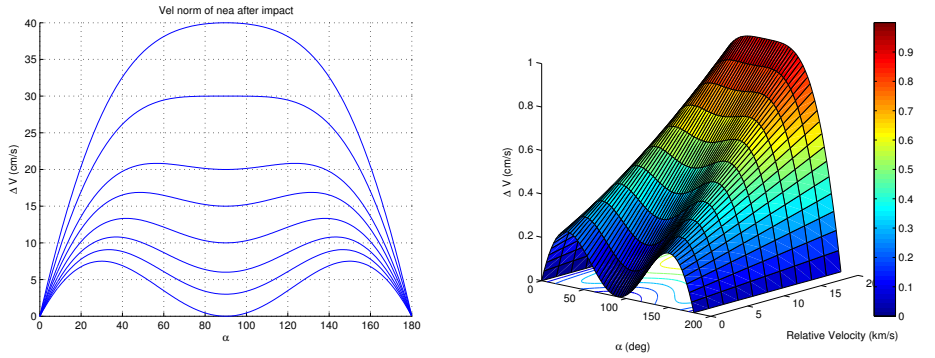

(a) Δv Imparted to NEA as a Function of Impact Angle, α for Varying Relative Impacting Velocities (b) Contour plot of Δv as a Function of α and Velocity of Impacting Spacecraft Relative to NEA

Figure 2. Behavior of the Optimal Impact Angle for Maximum Change in NEA Velocity

These results inform our understanding of what impact geometries will tend to maximize the change in a NEA's velocity and thereby *tend* to maximize the deflection of a NEA's orbit. However, we have not allowed the point along the NEA's orbit at which the impact occurs to vary. In future work, we may attempt to perform a direct analytical optimization of the deflection of a NEA's orbit as a function of both the impact direction of the spacecraft and the time of impact relative to a reference epoch, which necessarily involves the point along the NEA's orbit at which the impact occurs.

DEFLECTION DUE TO IMPACT

During an actual scenario in which a NEA is on a collision course with Earth, the most appropriate way to measure the deflection of the NEA is to difference the NEA's undeflected closest approach distance to Earth, which will be less than one Earth radius if the NEA's undeflected motion results in Earth collision, and the NEA's closest approach to Earth on the post-deflection orbit. However, for a deflection test scenario there is no collision or close approach to Earth with which to compute the aforementioned difference. Therefore, in a test scenario the deflection of the NEA's orbit is

computed by differencing the NEA's heliocentric position vector on its post-deflection orbit with what its heliocentric position vector would have been on the undeflected orbit after some amount of time has elapsed.

We present two models that can be used to compute the amount by which a NEA's orbit is deflected after a certain amount of time has elapsed. One is an accurate model based on Kepler's equation* and the other is an approximate model based on Gauss' form of the Lagrange Planetary equations. The latter method was proposed by Koenig[6] to compute the deflection when the impact occurs along the NEA's velocity direction at perihelion. We build upon this work by developing a computationally efficient approximate deflection equation that is valid at any point along the NEA's orbit with any impact angle in the NEA's orbit plane.

Approximate Deflection via Gauss' Form of the Lagrange Planetary Equations

The change in semi-major axis of a NEA's orbit due to a perturbation is given by[7]

$$\frac{\mathrm{d}a}{\mathrm{d}t} = \frac{2}{\sqrt{1-e^2}}\sqrt{\frac{a^3}{\mu_s}}\left[e\sin\nu\hat{F}_r + (1+e\cos\nu)\hat{F}_i\right] \tag{23}$$

where a is the NEA's undeflected heliocentric semi-major axis, μ_s is the Sun's gravitational parameter, e is the NEA's orbital eccentricity, ν is the NEA's true anomaly at the time of impact, and $\hat{F}_r$ and $\hat{F}_i$ are the components in the $\hat{\mathbf{r}}$ and $\hat{\mathbf{i}}$ directions, respectively, of an external force per unit mass applied to the NEA. An impulsive change in velocity due to an external force per unit mass is given by $\Delta\mathbf{v} = \int \hat{\mathbf{F}}\mathrm{d}t$. Taking the integral of Eq. (23) and the limit as $\mathrm{d}t \to 0$, the change in semi-major axis is computed as

$$\Delta a = \int_t^{t+\mathrm{d}t} \mathrm{d}a = \frac{2}{\sqrt{1-e^2}}\sqrt{\frac{a^3}{\mu_s}}\left[e\sin\nu\Delta v_{\hat{r}} + (1+e\cos\nu)\Delta v_{\hat{i}}\right] \tag{24}$$

We now need to relate the change in semi-major axis to a change in the NEA's position over time. We begin with the equation for the period of the NEA's orbit, T, as a function of its semi-major axis $T = 2\pi\sqrt{\frac{a^3}{\mu_s}}$. Taking the derivative of T with respect to a yields

$$\frac{\Delta T}{T} = 1.5\frac{\Delta a}{a} \tag{25}$$

Assuming a linear approximation, the deflection (magnitude of change in position vector) obtained one orbit period after the impact is $\Delta r_1 = \frac{\Delta T}{T}C$, where C is the approximate circumference of an ellipse, given by Ramanujan as[6,8]

$$C \approx \pi(a+b)\left(1 + \frac{3x^2}{10+\sqrt{4-3x^2}}\right) \tag{26}$$

where $x = (a-b)(a+b)$ and b is the semi-minor axis of the NEA's orbit. Since we are making a linear approximation, we can now write the following equation for the approximate deflection of the NEA's orbit at an arbitrary time Δt after the impact

$$\Delta r = \frac{\Delta t}{T}\Delta r_1 = 1.5\ C\ \frac{\Delta a}{a}\frac{\Delta t}{T} \tag{27}$$

*It is important to note that NEA orbits, like most orbits in nature, are *not* purely Keplerian. Perturbing forces such as solar radiation pressure, the Yarkovsky effect (anisotropic thermal re-radiation), and the gravity of planets cause gradual changes in the shape, size, and orientation of NEA orbits. However, here we are considering time spans of 2 years, and that generally amounts to ≤ 2 NEA orbit periods. Thus, treating the NEA orbit as Keplerian over that time span, strictly for the purposes of computing deflection, is sufficiently accurate for the purposes of our study.

True Deflection via Propagation with Kepler's Equation

The true* deflection of the NEA's orbit can be computed by propagating the new state of the NEA after impact, propagating the undeflected state of the NEA, and then differencing the deflected and undeflected states at a particular epoch subsequent to the time of impact. Performing these propagations by solving Kepler's equation yields sufficient accuracy for modest computational cost.

The heliocentric inertial $\Delta\mathbf{v}$ due to the impact is applied impulsively to the NEA's heliocentric inertial state vector, which is then transformed to classical Keplerian orbital elements. Kepler's equation is then solved to advance the deflected state, in orbital element space, to the desired time after impact, $t_{imp} + \Delta t$. The NEA state on the deflected orbit is then transformed from orbital element space at $t_{imp} + \Delta t$ to Cartesian space to yield the heliocentric position vector of the NEA on the deflected orbit (denoted by $^+$) at the desired post-impact time. This procedure is summarized in Eq. (28).

$$\mathbf{X}^+(t_{imp}) = \begin{bmatrix} \mathbf{r}_{nea} \\ \mathbf{v}^-_{nea} + \boldsymbol{\Delta}\mathbf{v} \end{bmatrix} \rightarrow \left[a^+,e^+,i^+,\Omega^+,\omega^+,\nu^+\right] \rightarrow \mathbf{r}^+_{nea}(t_{imp}+\Delta t) \tag{28}$$

The same procedure is then applied to compute the undeflected, denoted by $^-$, position vector of the NEA at $t_{imp} + \Delta t$, as summarized in Eq. (29).

$$\mathbf{X}^-(t_{imp}) = \begin{bmatrix} \mathbf{r}_{nea} \\ \mathbf{v}^-_{nea} \end{bmatrix} \rightarrow \left[a^-,e^-,i^-,\Omega^-,\omega^-,\nu^-\right] \rightarrow \mathbf{r}^-_{nea}(t_{imp}+\Delta t) \tag{29}$$

Finally, the deflection is calculated by computing the magnitude of the difference of the deflected and undeflected NEA position vectors at $t_{imp} + \Delta t$ as shown in Eq. (30).

$$\Delta r = \|\mathbf{r}^+_{nea}(t_{imp} + \Delta t) - \mathbf{r}^-_{nea}(t_{imp} + \Delta t)\| \tag{30}$$

Figure 7(c) shows the true and approximate deflections computed over time for the example case of NEA 2010 GZ_{33}. The two solution methods agree rather well at the 2 year mark. However, the difference between the results of the two methods becomes more significant after the NEA's first post-deflection perihelion passage. These deviations are such that the approximate method sometimes underestimates the true deflection and sometimes overestimates it, thereby providing a reasonable estimate over time. As time increases, the major trend is that the approximate method tends to underestimate the true deflection. We therefore have a good expectation of indeed obtaining a measurable deflection of a NEA's orbit if the approximate method predicts a measurable deflection.

PARAMETERS AND CONSTRAINTS

In this section we provide a brief overview of the NEAs we used in this study, along with the parameters and constraints used for the trajectory design. To begin, NEAs are classified into four groups based on their orbital characteristics:†

1. *Amors* have orbits exterior to Earth's. The perihelion of an Amor's orbit is therefore between 1.017 and 1.3 AU. There were 3017 Amors known at the time of our study.

*As noted previously, here we are neglecting natural environmental perturbations on the NEA's orbit because we are interested in time spans of $\leq$ 2 NEA orbit periods.

†`http://neo.jpl.nasa.gov/neo/groups.html`. Last accessed on 01/23/2012.

2. *Apollos* are Earth-crossing NEAs with semi-major axes larger than Earth's (> 1 AU), but with perihelia less than 1.017 AU. There were 4392 Apollos known at the time of our study and they continue to comprise the majority of the currently known NEA population.

3. *Atens* are Earth-crossing NEAs, with semi-major axes smaller than Earth's (< 1 AU), but with aphelia greater than 0.983 AU. There were 660 Atens known at the time of our study.

4. *Atiras* have orbits inside of Earth's and therefore have aphelia less than 0.983 AU. There are currently only 11 known Atiras. It is possible that many more exist but are difficult to find using ground-based observatories since Atiras spend most of their orbits in our daytime sky.

Apollos and Atens tend to be more accessible, in terms of low total mission Δv, to spacecraft missions because they are Earth-crossing NEAs and their orbits are often rather similar to Earth's orbit. However, for our study we selected only Amor and Atira NEAs as candidate mission targets specifically because their orbits are either completely exterior or interior to Earth's orbit. This ensures that Earth will never be threatened by deflection system testing activities, regardless of what might go wrong during the the test missions. Additionally, we imposed the constraint of heliocentric orbit inclination $\leq 20°$ in the interests of keeping mission Δv manageable.* Thus, the candidate target NEAs for our study consist of the 2185 Amor and Atira NEAs with inclination $\leq 20°$—of these, only 5 are Atiras. Table 1 compares our selected population of candidate NEAs to the known population at the time of our study†, and Figure 3 shows the relationship between heliocentric orbit eccentricity and semi-major axis for all of these NEAs.

Table 1. NEAs Selected for This Study

Type	Known	Selected
Amors	3017	**2180**
Apollos	4392	0
Atens	660	0
Atiras	11	**5**
Total	8080	**2185**

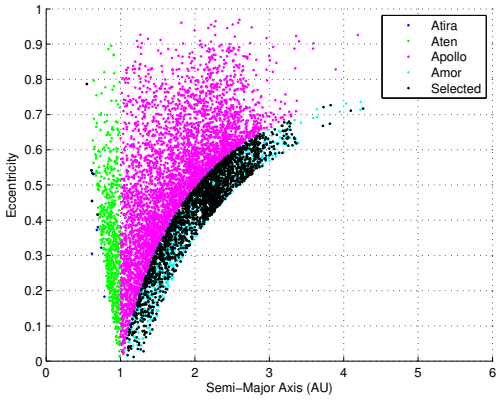

Figure 3. Eccentricity vs. Semi-major Axis for the NEA Population

The methodology we developed for our analysis was inspired by the Near-Earth Object (NEO) Human Space Flight (HSF) Accessible Targets Study (NHATS), which utilizes broad trajectory survey techniques to identify all NEAs which offer round-trip trajectory opportunities within a specific

*The fact that heliocentric orbit plane change is often one of the largest drivers of total mission Δv is a well-known consequence of astrodynamics.

†The list of NEAs was obtained from the JPL Small-Body Database (SBDB) Search Engine, `http://ssd.jpl.nasa.gov/sbdb_query.cgi`, on 06/30/2011, and the corresponding ephemeris files were then obtained from the JPL HORIZONS system, `http://ssd.jpl.nasa.gov/?horizons`.

performance envelope.[9] In our case, we designed an algorithm that uses a trajectory grid scan technique to assess the suitability of each candidate NEA by computing all possible trajectories to the NEA for both the observer (rendezvous) and impactor (intercept) separately. A schematic of the parameter space structure of this algorithm is provided in Figure 4.

The algorithm varies two independent parameters, departure date and Time of Flight (TOF), within set bounds and uses a Lambert solver to compute the associated rendezvous or intercept trajectory Δv requirements for each combination of departure date and TOF. The constraints applied within the algorithm are summarized in Table 2. For the purposes of mission mass calculations, we assume the use of launch vehicles from the Atlas V family so that no new launch vehicles would be required for the deflection test missions that we design—this should help make the proposed deflection test missions affordable. Two-body dynamics, with the Sun as the central body, and the method of patched conics are assumed for the spacecraft, since a Lambert solver is used for the trajectory design, while high-fidelity ephemerides are used for the Earth and NEAs. We also enforced the constraint that the observer spacecraft must arrive between 3 months and 3 years prior to the impactor's collision with the NEA in order to provide the observer spacecraft adequate time to gather data on the NEA prior to the impact. Since the observer is able to study the NEA both before and after the impact, it will be able to collect a wealth of data on the NEA's pre- and post-impact state, thus facilitating accurate characterization of the effects of the kinetic impact.

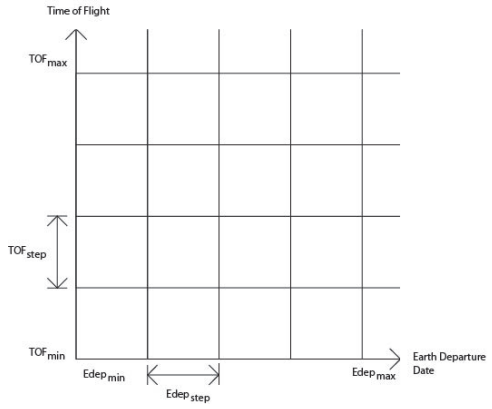

Figure 4. Trajectory Grid Schematic

Table 2. Trajectory Constraints for the Observer and Impactor Spacecraft

	Observer	Impactor
Dep. Date	2016 - 2026	2016 - 2026
Arr. Date	$t_{arr_{imp}} - 3$ yr. $\leq t_{arr_{obs}}$ $t_{arr_{obs}} \leq t_{arr_{imp}} - 3$ mon.	–
TOF (days)	≤ 1000	≤ 1000
C_3 (km^2/s^2)	≤ 60	≤ 60
Δv_{tot} (km/s)	≤ 7.0	–
mass$_{dry}$ (kg)	≥ 500	–

Besides safety and affordability, an additional constraint is that the deflection imparted to the NEA by the kinetic impactor must be easily measured by the observer spacecraft. Since a NEA's orbit can generally be determined to within several km or less when a transponder-equipped spacecraft is near the NEA, we require that the deflection of the NEA's orbit be at least 100 km by 2 years after the time of impact to ensure a measurable deflection experiment.

In order to compute the amount by which a NEA is deflected due to an impact, the NEA's mass must be known. However, the mass of a NEA must generally be measured by a spacecraft and so masses are not known for the vast majority of the NEA population. We therefore use the following method to estimate the masses of the NEAs for study. We assume a spherical shape for each NEA, which allows the NEA's mass, M, to be computed as

$$M = \rho \frac{4}{3} \pi \left(\frac{D}{2}\right)^3 \tag{31}$$

where D is the estimated diameter of the NEA and ρ is its assumed density. The density of a NEA will generally range between 1.3 and 8 $\mathrm{g/cm^3}$, although the likely value for the density of many NEAs is about 2.6 $\mathrm{g/cm^3}$, so we assume this density for the NEAs in our study. A NEA's estimated diameter, in units of km, is computed using its absolute magnitude (a measure of optical brightness), H, and an assumed geometric albedo (indicative of surface reflectivity), p, according to[10]

$$D = \frac{1329}{\sqrt{p}} 10^{-0.2H} \tag{32}$$

For most NEAs, p will generally range between 0.05 and 0.25, so we use the average value of 0.15 for our study. The value of H for each NEA is obtained from the Jet Propulsion Laboratory (JPL) Small-Body Database (SBDB) Search Engine*.

In our analysis we considered only NEAs with estimated diameters $\geq$ 95 m as it may be difficult for the terminal guidance systems on the observer and impactor spacecraft to successfully locate, identify, and track NEAs with smaller diameters. A detailed analysis of the minimum NEA diameter that can be handled by an impactor is beyond the scope of our study and has been relegated to future work. Of the 2185 NEAs first identified in our analysis, 1556 have estimated diameter $D \geq 95$ m.

TRAJECTORY DESIGN AND RESULTS

The aforementioned 1556 NEAs with $D \geq 95$ m and inclination $\leq 20^\circ$ from the Amor and Atira groups were first subjected to rendezvous trajectory processing using the previously described trajectory grid scanning methods. An Atlas V 401 launch vehicle was assumed for the purposes of computing initial total spacecraft wet mass as a function of Earth departure C_3. The launch payload mass performance as a function of C_3 for the Atlas V 401 and 551 launch vehicles is shown in Figure 5.†

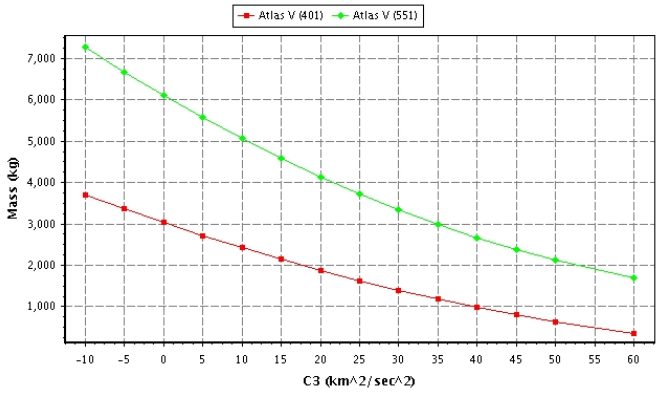

Figure 5. Payload Mass Performance for the Atlas V 401 and 551 Launch Vehicles

Of the 1556 NEAs analyzed in this way, 450 NEAs offer at least one rendezvous trajectory solution that satisfies the $\Delta v_{tot} \leq 7$ km/s constraint set forth for the observer spacecraft in Table 2.‡ These trajectory solutions also satisfy the observer spacecraft constraint in Table 2 stating that the

*`http://ssd.jpl.nasa.gov/sbdb_query.cgi`. Last accessed on 01/15/2012.

†These data were obtained from `http://elvperf.ksc.nasa.gov/elvMap/`. Last accessed on 01/15/2012.

‡Here we define the total Δv as the sum of the magnitude of the change in velocity required to depart a reference circular Earth parking orbit and the magnitude of the change in velocity required to match the NEA's orbit velocity upon arrival. Although the asymptotic declination angle associated with Earth departure is not considered, note that the launch

final mass of the observer upon NEA arrival must be $\geq$ 500 kg, based on the aforementioned mass performance of the Atlas V 401 and an assumed observer spacecraft thruster specific impulse of 300 seconds. This final mass constraint was selected to ensure that the observer spacecraft would be sufficiently capable. The 450 NEAs identified at this stage of the analysis were used as the initial population for subsequent analyses that incorporate the impactor spacecraft.

We next surveyed mission opportunities for three types of observer/impactor scenarios. In the first scenario the observer and impactor spacecraft are launched separately, each on its own Atlas V 401 launch vehicle. In the second scenario, the observer and impactor are co-manifested on a single Atlas V 551 launch vehicle that directly injects the combined observer/impactor spacecraft stack into the interplanetary trajectory bound for rendezvous with the NEA. The observer spacecraft coasts on this trajectory until NEA arrival, but the impactor spacecraft separates prior to NEA arrival and performs a maneuver such that it impacts the NEA after the arrival of the observer. In the third scenario, the observer and impactor spacecraft are co-manifested on a single Atlas V 401 launch vehicle that deposits both vehicles into a low circular Earth parking orbit. From this common orbit, the observer and impactor then depart Earth separately using their own propulsion systems at different times. The constraints specified in Table 2 are enforced for all of these scenarios.

Assuming that Table 2 constraints are met, a trajectory solution set for the observer and impactor is considered viable if the approximate deflection, Δr of the NEA's orbit after $\Delta t = 2$ years is $\geq$ 100 km, as described previously. Recall that the approximate method for computing Δr, given by Eqs. (23)–(27) is used to make the overall computational burden tolerable. In the tables of results that follow, we present the top ranking NEAs in terms of the maximum Δr mission solution they offer. However, note that all of these NEAs offer multiple viable solutions and only their extremal solutions are tabulated herein.

Two-Launch Scenario

Using the Atlas V 401 as the launch vehicle for both the observer and impactor, a total of 263 NEAs with an assumed diameter $D \geq 95$ m were found to offer at least one trajectory solution that meets the the constraints specified in in Table 2. Of these, a total of 148 NEAs were found to offer at least one observer/impactor trajectory solution set with an achieved $\Delta r \geq 100$ km after 2 years, with an assumed β of 1. With $\beta = 2.5$, 180 NEAs offered at least one mission solution with $\Delta r \geq 100$ km after 2 years. Achieved Δr for these sets of NEAs is plotted versus NEA diameter in Figure 6. As expected, the larger achieved deflections tend to be obtained for the less massive NEAs, and increased β dramatically improves achieved deflection performance, allowing the 2-year Δr requirement to be met with considerably larger NEAs. This underscores the importance of properly characterizing β.

Table 3 shows the top 5 NEAs, selected and ranked according to maximum achieved Δr, and the maximum Δr observer/impactor solution set is shown for each NEA. Note that only the optimal Δr observer/impactor mission solution for each NEA is shown, however, each of these NEAs offers multiple viable mission solutions.

Table 4 shows the top 5 NEAs after further constraints are introduced into the analysis such that the mission must depart Earth between the years 2016 and 2020, and only NEAs with an Orbit

vehicle performance data in Figure 5 assume a declination of $\pm 28.5^\circ$, which is commensurate with a launch from the NASA Kennedy Space Center. Incorporating the asymptotic Earth departure declination angle into our study has been identified as a future work item.

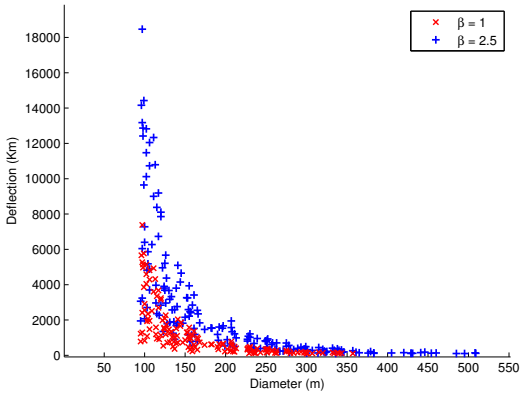

Figure 6. Approximate Deflection (km) after 2 years vs. Diameter (m) for Candidate Target NEAs with $\beta = 1$ and $\beta = 2.5$

Table 3. Top 5 NEAs for the Two-Launch Scenario in Descending Order of Maximum Approximate Deflection, Assuming $\beta = 1$

	D (m)	OCC	Type	Dep Date	TOF (days)	TBI (days)	C_3 (km^2/s^2)	ΔV_{arr} (km/s)	ΔV_{tot} (km/s)	m_{final} (kg)	Δr (km)
1	2011 GQ_{59}		Obs	2020-4-18	824	134	38.1	2.14	6.98	511	
	97	5	Imp	2021-9-13	445		12.54	17.99		2,279	7,122
2	2001 DS_8		Obs	2017-1-29	845	177	40.22	1.18	6.11	655	
	99	6	Imp	2018-7-8	497		16.5	18.87		2,057	5,621
3	2007 EO		Obs	2018-4-4	715	107	39.34	1.1	5.99	695	
	96	5	Imp	2019-8-18	321		5.55	11.64		2,696	5,425
4	2011 AS_{26}		Obs	2018-1-25	710	206	38.86	1.97	6.84	527	
	97	5	Imp	2019-6-11	414		12.58	13.8		2,277	5,030
5	2007 VH_3		Obs	2025-1-19	687	234	37.06	1.17	5.97	737	
	98	5	Imp	2026-6-18	406		10.67	14.19		2,388	4,969

Condition Code (OCC) ≤ 4 are considered. The OCC is a measure of how well a NEA's orbit is known, with 0 representing extremely good knowledge of the NEA's orbit and 9 representing extremely poor orbit knowledge.* Additional details for these solutions are presented in Table 5, including the magnitude of the Δv imparted to the NEA by the impactor, the change in the semi-major axis of the NEA's orbit, Δa, the true deflection of the NEA when 2 perihelion passages have occurred following the impact ($\Delta t = 2T_p$), and the energy per unit mass (i.e., the specific energy), E_{spec}, deposited into the NEA by the impactor. Note that specific energies on the order of 10^2 J/kg would most likely be required to shatter a NEA. Since the values in Table 5 are smaller than this by more than several orders of magnitude it is very likely that the deflection experiments being modeled here would have little chance of fragmenting the NEAs.

Two contour plots showing all observer/impactor solutions for the top NEA in Table 4, 2010 GZ_{33}, are shown in Figure 7(a) and 7(b). These plots show the 2-year approximate deflection and observer spacecraft final mass, respectively, as functions of the impactor's Earth departure date and TOF to NEA intercept. The maximum deflection shown in Figure 7(a) is 2665 km, which coincides with the results in Table 4. Figure 7(c) presents the true and approximate deflection

*OCC is also known as the Minor Planet Center (MPC) "U" parameter and a detailed technical explanation is found at `http://www.minorplanetcenter.net/iau/info/UValue.html`. Last accessed on 01/15/2012.

Table 4. Top 5 NEAs for the Two-Launch Scenario in Descending Order of Maximum Approximate Deflection, Assuming $\beta = 1$, Departure Year Constrained to 2016-2020, and Only Considering NEAs with OCC ≤ 4

	D (m)	OCC	Type	Dep Date	TOF (days)	TBI (days)	C_3 (km^2/s^2)	ΔV_{arr} (km/s)	ΔV_{tot} (km/s)	m_{final} (kg)	Δr (km)
1	2010 GZ_{33}		Obs	2018-6-13	167	890	38.56	2.04	6.9	520	
	117	4	Imp	2019-12-23	499		18.84	17.69		1,931	2,665
2	2002 QE_{47}		Obs	2017-11-15	537	377	32.92	0.94	5.58	917	
	139	1	Imp	2019-5-5	378		8.61	12.54		2,510	1,477
3	2008 CD_{22}		Obs	2016-2-20	296	398	36.61	2.18	6.96	531	
	131	0	Imp	2017-4-30	259		16.24	8.46		2,071	1,277
4	2008 SR		Obs	2017-11-15	639	242	34.68	1.83	6.54	639	
	153	4	Imp	2019-4-12	368		7.82	12.44		2,558	1,246
5	1998 KG_3		Obs	2017-10-23	166	457	13.02	1.03	4.84	1,584	
	123	0	Imp	2018-8-12	330		8.58	7.61		2,512	542

Table 5. Additional Results for the Top 5 NEAs Shown in Table 4

	NEA	D (m)	OCC	Dep. Date	ΔV (cm/s)	Δa (km)	Δr (km)	$\Delta r(2T_p)$ (km)	$2T_p$ (year)	E_{spec} (J/kg)
1	2010 GZ_{33}	117	4	2019-12-23	1.23	392.77	2,665	11,688	5.06	$1.39e^{-4}$
2	2002 QE_{47}	139	1	2019-5-5	0.63	200.81	1,477	5,582	4.77	$5.37e^{-5}$
3	2008 CD_{22}	131	0	2017-4-30	0.50	137.59	1,277	3,619	3.96	$2.44e^{-5}$
4	2008 SR	153	4	2019-4-12	0.50	195.62	1,246	5,676	5.52	$4.04e^{-5}$
5	1998 KG_3	123	0	2018-8-12	0.29	36.04	542	769	2.26	$2.85e^{-5}$

of this NEA as a function of time. Figure 7(d) shows the trajectory solutions for observer and impactor, corresponding to the maximum Δr solution given in Table 4. An interesting feature of this solution is that the maximum Δr solution does not have the impactor striking the NEA at the NEA's perihelion.

One-Launch Scenario: Direct Injection

After analyzing the two-launch scenario, we considered the one-launch scenario, which consists of the observer and impactor spacecraft co-manifested on a single Atlas V 551 launch vehicle that directly injects the observer/impactor spacecraft stack into a hyperbolic Earth departure trajectory. Some time later, the impactor separates from the observer and performs a maneuver that leads to a later impact while the observer spacecraft continues coasting to the NEA and arrives prior to the impactor. This is done such that the constraints in Table 2 are satisfied.

The nominal Earth departure trajectory is taken to be the minimum Δv_{tot} trajectory for the observer spacecraft to rendezvous with the NEA after a TOF t_0 has elapsed, following the Earth departure date—this is the black trajectory depicted in Figure 8. This trajectory solution was initially found for each NEA using the grid search method outlined previously in Figure 4. After time t_1 has elapsed, a maneuver $\mathbf{\Delta V}_1$ is performed such that the impactor spacecraft departs on a separate trajectory leading to intercept of the NEA some time after observer arrival—this trajectory is shown in red in Figure 8. The optimization scheme is written such that a second maneuver by the impactor, $\mathbf{\Delta V}_2$, is permitted after a time t_2 has elapsed if it serves to improve overall performance. Following this optional second impactor maneuver, the impactor intercepts the NEA after a time t_3 elapses.

The optimization scheme is written such that the objective is to maximize the deflection of the

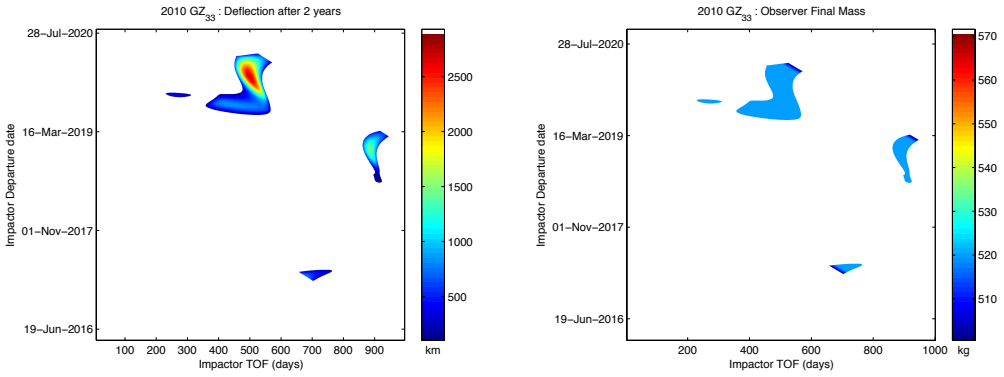

(a) Achieved 2-year Δr as a Function of Impactor Departure Date and TOF

(b) Achieved Observer Final Mass at NEA Arrival as a Function of Impactor Departure Date and TOF

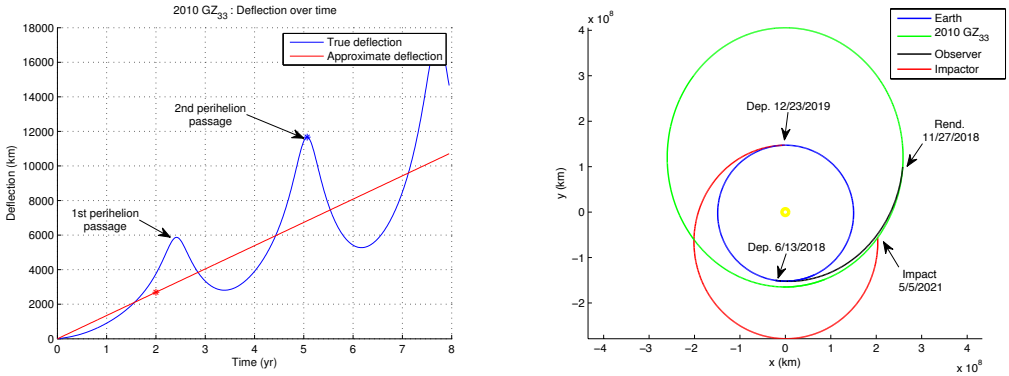

(c) True and Approximate Deflection of NEA vs. Time

(d) Optimal Trajectory Solution Set for Observer and Impactor

Figure 7. Optimal Observer/Impactor Solution Set Data for NEA 2010 GZ_{33}

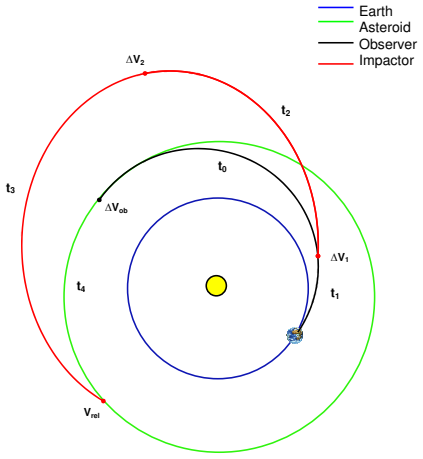

Figure 8. Direct one-launch scenario schematic

NEA's orbit. Accordingly, the performance index, J, is defined as

$$J = \max \|\mathbf{\Delta r}\| \tag{33}$$

with variables

$$\mathbf{X}_p = \left[\begin{array}{cccccc} t_1 & t_2 & t_3 & t_4 & \mathbf{\Delta v}_{1_{imp}} & \mathbf{\Delta v}_{2_{imp}} \end{array} \right]^T \tag{34}$$

The equality and inequality constraints are

1. $\mathbf{r}_{imp} = \mathbf{r}_{nea}(t_0 + t_4)$ at time of impact
2. 3 months $\leq t_4 \leq 3$ years
3. Impactor mass $m_{imp_{dry}} > 0$ at intercept
4. $\|\mathbf{\Delta r}\| \geq 100$ km after 2 years

The third constraint is necessary because the total initial spacecraft mass (observer + impactor) is limited by the launch vehicle performance. The observer dry mass, $m_{obs_{dry}}$, is set to 500 kg, a thruster specific impulse, I_{sp}, of 300 seconds, corresponding to nominal hypergolic bipropellant propulsion system performance, is assumed for both the observer and the impactor, and the total launch mass, m_{C_3}, is determined as a function of the Earth departure C_3 from the Atlas V 551 launch vehicle performance data shown in Figure 5. The dry mass of the impactor, $m_{imp_{dry}}$, is computed using the ideal rocket equation,

$$\frac{m_{imp_{wet}}}{m_{imp_{dry}}} = \mathrm{e}^{\frac{\Delta v_{imp}}{gIsp}} \tag{35}$$

where $m_{imp_{wet}} = m_{C_3} - m_{obs_{wet}}$, $m_{obs_{wet}} = m_{obs_{dry}} \mathrm{e}^{\frac{\Delta v_{2_{obs}}}{gIsp}}$, and $\Delta v_{2_{obs}}$ is the rendezvous Δv for the observer. Once the dry mass of the impactor spacecraft is computed, the Δv imparted to the NEA can be calculated via Eqs. (12)–(18), which then allows calculation of the NEA deflection, Δr, using Eqs. (23)–(27).

With the foregoing scheme for computing the optimal one-launch NEA deflection solution, and assuming an Atlas V 551 launch vehicle, a total of 68 NEAs were found to offer at least one direct one-launch mission solution that satisfies all the constraints listed in Table 2 and achieves $\Delta r \geq 100$ km after 2 years. Note that the 67 NEAs were found by using $\beta = 1$, which is the least optimistic choice for β. If β is > 1, it is quite likely that more NEAs would offer viable mission solutions. As an example, Figure 9(a) shows the optimal solution set for NEA 2004 KE_1, one of the top 5 candidate NEAs for the direct one-launch scenario listed in Table 6.

One Launch Scenario: Staging in Low Earth Orbit (LEO)

The final scenario we examined involves launching the observer and impactor to a 500 km altitude circular LEO, from which the two spacecraft depart at different times. The viable observer/impactor trajectory solution sets identified for the previously discussed two-launch scenario are used as the initial candidate trajectories for the single launch to LEO analysis.

The maximum amount of mass that an Atlas V 401 can deliver to a 500 km circular LEO at an inclination of 28.5° is $m_{max} = 8760$ kg*. Therefore, the total combined initial observer/impactor

*`http://elvperf.ksc.nasa.gov/elvMap/`.

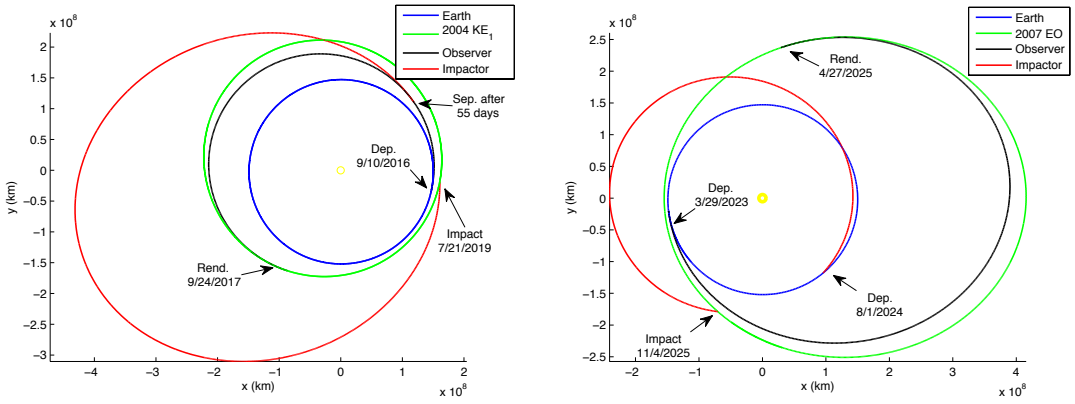

(a) One-Launch Direct to 2004 KE_1 using Atlas V 551 (b) One-Launch to LEO to 2007 EO using Atlas V 401

Figure 9. Optimal One-Launch Trajectory Solution Sets for the NEAs 2004 KE_1 and 2007 EO

Table 6. Top 5 NEAs for the Direct Single Launch Scenario in Descending Order Approximate NEA Diameter, Assuming $\beta = 1$

	NEA	D (m)	OCC	Type	Dep. Date	C_3 (km^2/s^2)	ΔV_{arr} (km/s)	TSP (days)	TOF (days)	TBI (days)	m_{final} (kg)	Δr (km)
1	2004 KE_1	162	0	Obs Imp	2016-9-10	7.70	1.38 7.71	55	379 989	665	500 923	151
2	1996 XB_{27}	159	0	Obs Imp	2027-3-20	7.84	1.01 9.24	20	207 852	665	500 947	173
3	2009 SC_{15}	158	5	Obs Imp	2023-3-20	22.42	0.41 6.11	10	270 985	725	500 875	148
4	1998 HG_{49}	156	0	Obs Imp	2018-11-4	7.16	1.00 8.62	35	313 868	590	500 955	181
5	2002 XU_4	139	2	Obs Imp	2022-12-2	29.99	1.78 9.81	15	174 984	825	500 523	138

wet mass in LEO can be no greater than m_{max}. Assuming an observer dry mass of $m_{obs_{dry}} = 500$ kg, the required observer wet mass is computed using the rendezvous trajectory Δv results as follows

$$m_{obs_{wet}} = m_{obs_{dry}} \mathrm{e}^{\frac{\Delta v_{obs_{dep}} + \Delta v_{obs_{arr}}}{gIsp}} \tag{36}$$

The impactor dry mass, $m_{imp_{dry}}$, is determined using the Atlas V 401 mass performance shown in Figure 5 and the $C_{3_{imp}}$ for Earth departure associated with the particular impactor trajectory solution under consideration. The required impactor wet mass at LEO departure is then

$$m_{imp_{wet}} = m_{imp_{dry}} \mathrm{e}^{\frac{\Delta v_{imp_{dep}}}{gIsp}} \tag{37}$$

For the trajectory solution set to be considered viable for the single launch to LEO scenario, the spacecraft wet masses must satisfy the constraint that $m_{imp_{wet}} + m_{obs_{wet}} \leq m_{max}$.

Table 7 shows only the top 5 optimal solutions in which the observer uses minimum Δv and the impactor achieves maximum approximate deflection, Δr. However, there are additional trajectory solution sets for each of these NEAs that satisfy all constraints. As an example, Figure 9(b) shows the optimal solution set for NEA 2007 EO, which is the top candidate shown in Table 7. These results demonstrate that the single launch to LEO scenario is a viable alternative.

Table 7. Top 5 NEAs for the Single Launch to LEO Scenario in Descending Order of Maximum Approximate Deflection, Assuming $\beta = 1$

	D (m)	OCC	Type	Dep Date	TOF (days)	TBI (days)	C_3 (km^2/s^2)	ΔV_{arr} (km/s)	m_{final} (kg)	Δr (km)
1	2007 EO		Imp	2024-8-1	460	191	38.48	17.51	1043	
	96	5	Obs	2023-3-29	760		45.78	0.53	500	2,805
2	2001 DS_8		Imp	2017-6-28	883	188	42.88	23.34	886	
	99	6	Obs	2017-1-29	845		40.22	1.18	500	2,799
3	2009 FB_5		Imp	2023-9-9	832	309	39.96	20.99	989	
	98	9	Obs	2023-4-5	680		37.57	1.00	500	2,592
4	2007 VH_3		Imp	2023-5-25	531	421	38.73	17.67	1,034	
	98	5	Obs	2022-1-11	609		39.75	0.78	500	2,550
5	2006 YD_{12}		Imp	2021-8-6	96	961	40.24	21.58	979	
	102	7	Obs	2017-1-25	789		42.85	0.81	500	2,293

CONCLUSION

Near-Earth asteroids (NEAs) have collided with Earth in the past and will do so in the future. These objects, therefore, pose a continuing threat to our species. It is imperative that we begin testing candidate NEA deflection systems, such as the kinetic impactor, on harmless NEAs now, so that we will be prepared before an eminent threat is discovered. In this paper, we have surveyed the known NEA population to determine which NEAs may be good targets for kinetic impactor deflection test missions by virtue of offering safe and affordable mission scenarios that are likely to yield a measurable deflection.

To facilitate this study, we developed new, more accurate mathematical models for the change in velocity imparted to a NEA by a kinetic impactor and the resulting change in the NEA's orbit over time. Our models account for any incoming impactor direction in three-dimensional space relative to the NEA, and allow for the impact to occur at any point along the NEA's orbit. This represents an improvement over previous work that restricts the incoming impactor direction to coincide with the NEA's heliocentric velocity direction and/or only considers impacts at the NEA's perihelion.

Our algorithms have identified 148 NEAs that offer at least one satisfactory trajectory solution utilizing two Atlas V 401 launch vehicles. In a single launch analysis utilizing an Atlas V 551 launch vehicle, 68 NEAs were found to offer at least one satisfactory trajectory solution. The mission scenarios we have designed for these NEAs all have Earth departure dates within the coming decade and therefore represent near-term opportunities for safe, affordable, and meaningful deflection test missions. These missions have the potential to provide humanity with the tools necessary to avert one of the deadliest natural disasters ever to affect our planet.

Future Work

Certain key assumptions were necessary to facilitate this study, and their effects should be explored in future work. One such assumption is the minimum diameter of 95 m for candidate target NEAs. Further analysis of terminal guidance system performance is required to truly ascertain the range of physical parameters that are acceptable for target NEAs. One issue is that the brightness of a NEA as seen in a spacecraft's camera depends simultaneously on a NEA's diameter, shape, and surface reflectivity, along with the angle between the Sun, NEA, and spacecraft during the final approach to impact or rendezvous. This problem requires sophisticated analysis on a per-NEA basis and is severely complicated by the lack of accurate physical data for the majority of the known NEA

population. This data deficiency may be addressed to some extent by a future space-based NEA survey telescope operating in infrared wavelengths, assuming that such a mission is ever launched.

Another aspect of this problem that would benefit from further analysis is the measurability of the deflection experiment. Simulation of the orbit determination process for a NEA with observer spacecraft telemetry before, during, and after the impact would permit refinement of the notional deflection measurability threshold utilized in this study (100 km after 2 years). Such a simulation would also permit analysis of the extent to which the $\Delta\mathbf{v}$ imparted to the NEA by the impactor can accurately be reconstructed. This has strong implications for our ability to accurately assess β.

The trajectory design and mission performance results provided herein can also be refined by rigorously accounting for the effects of asymptotic departure declination angle associated with the Earth departure maneuvers to reach the NEA. Another issue is that the plane of the Earth parking orbit will precess under the influence of perturbations, chiefly the J_2 non-spherical gravity term. This complicates the timing for the mission sequence and can yield narrow Earth departure windows.

A different approach may also be taken to ensure the safety of NEA deflection experiments. In this study we addressed safety by selecting only NEAs whose orbits are entirely interior or exterior to Earth's orbit. In future work we may examine pre- and post-deflection NEA trajectories in a circular or elliptic Sun-Earth Restricted Three-Body Problem (RTBP). This would allow deflected NEA trajectories to be made safe by enclosing Earth in zero-velocity curves.

Finally, the analytical optimization of impact angle for maximizing the Δv imparted to a NEA may be made more general by including the elevation angle, δ. The analysis may also be extended by including the orbital dynamics and recasting the problem such that the deflection of the NEA's orbit becomes the performance index and the time of kinetic impact, prior to a some reference epoch, becomes an additional control parameter, thereby accounting for the NEA's true anomaly.

ACKNOWLEDGMENT

This work was performed as a summer internship funded by NASA HQ and the NASA Goddard Space Flight Center's Exploration Systems Projects Office.

REFERENCES

[1] B. Wie, "Astrodynamic Fundamentals for Deflecting Hazardous Near-Earth Objects," *60th International Astronautical Congress, IAC-09-C1.3.1*.

[2] M. G. Schaffer, A. C. Charania, and J. R. Olds, "Evaluating the Effectiveness of Different NEO Mitigation Options," *Planetary Defense Conference, AIAA 2007-P2-1*, Washington, D.C., March 2007.

[3] J. P. Sanchez and *et al.*, "Multicriteria Comparison Among Several Mitigation Strategies for Dangerous Near-Earth Objects," *Journal of Guidance, Control, and Dynamics*, Vol. 32, January-February 2009.

[4] B. Kaplinger, B. Wie, and J. Basart, "A Preliminary Study on Nuclear Standoff Explosions for Deflecting Near-Earth Objects," *1st IAA Planetary Defense Conference*, Granada, Spain, April 2009.

[5] K. A. Holsapple, "The Scaling of Impact Processes in Planetary Science," *Annual Review of Earth and Planetary Sciences*, Vol. 21, May 1993, pp. 333–373.

[6] J. D. Koenig and C. F. Chyba, "Impact Deflection of Potentially Hazardous Asteroids Using Current Launch Vehicle," *Science and Global Security*, No. 15, 2007, pp. 57–83.

[7] B. D. Tapley, B. E. Schutz, and G. H. Born, *Statistical Orbit Determination*. Elsevier Inc., 2004.

[8] M. B. Villarino, "Ramanujan's Perimeter of an Ellipse," *ArXiv Mathematics e-print*, February 2008.

[9] B. W. Barbee, R. G. Mink, D. R. Adamo, and C. M. Alberding, "Methodology and Results of the Near-Earth Object (NEO) Human Space Flight (HSF) Accessible Targets Study (NHATS)," *Advances in the Astronautical Sciences*, Vol. 142, San Diego, CA, Univelt, Inc., 2011, pp. 613–632.

[10] S. R. Chesley and *et al.*, "Quantifying the Risk Posed by Potential Earth Impacts," *Icarus*, Vol. 159, October 2002, pp. 423–432. doi:10.1006/icar.2002.6910.